Department of Pathology, Anatomy, and Cell Biology Faculty Papers

Department of Pathology, Anatomy, and Cell Biology

11-22-2004

Control of mitochondrial motility and distribution by the calcium signal: a homeostatic circuit.

Muqing Yi
Thomas Jefferson University

David Weaver
Thomas Jefferson University

György Hajnóczky
Thomas Jefferson University

Control of mitochondrial motility and distribution by the calcium signal: a homeostatic circuit

Muqing Yi, David Weaver, and György Hajnóczky

Department of Pathology, Anatomy, and Cell Biology, Thomas Jefferson University, Philadelphia, PA 19107

Mitochondria are dynamic organelles in cells. The control of mitochondrial motility by signaling mechanisms and the significance of rapid changes in motility remains elusive. In cardiac myoblasts, mitochondria were observed close to the microtubular array and displayed both short- and long-range movements along microtubules. By clamping cytoplasmic $[Ca^{2+}]$ ($[Ca^{2+}]_c$) at various levels, mitochondrial motility was found to be regulated by Ca^{2+} in the physiological range. Maximal movement was obtained at resting $[Ca^{2+}]_c$ with complete arrest at 1–2 μM. Movement was fully recovered by returning to resting $[Ca^{2+}]_c$, and inhibition could be repeated with no apparent desensitization. The inositol 1,4,5-trisphosphate– or ryanodine receptor-mediated $[Ca^{2+}]_c$ signal also induced a decrease in mitochondrial motility. This decrease followed the spatial and temporal pattern of the $[Ca^{2+}]_c$ signal. Diminished mitochondrial motility in the region of the $[Ca^{2+}]_c$ rise promotes recruitment of mitochondria to enhance local Ca^{2+} buffering and energy supply. This mechanism may provide a novel homeostatic circuit in calcium signaling.

Introduction

Until recently, mitochondria were envisioned to serve as cellular power plants, but current research has also revealed mitochondria as fundamental elements in intracellular signaling. Among other contributions, mitochondria play a role in shaping calcium signals (for reviews see Duchen, 2000; Rizzuto et al., 2000, 2004; Hajnóczky et al., 2002; Petersen, 2002; Parekh 2003) and serve as the integration site of cell survival and death-promoting signals in many paradigms of apoptosis and necrosis (for reviews see Kroemer and Reed, 2000; Bernardi et al., 2001; Jacobson and Duchen, 2001; Martinou and Green, 2001; Demaurex and Distelhorst, 2003; Scorrano and Korsmeyer, 2003). Evidence has also been emerging that mitochondria need to be strategically localized at particular subcellular sites both for providing energy supply and for participating in intracellular signaling (Park et al., 2001). For example, a close association between subdomains of the ER and mitochondrial surface appears to be necessary for the propagation of ER Ca^{2+} release to the mitochondria (Rizzuto et al., 1993; 1998; Csordás et al., 1999), close associations between subdomains of the plasma membrane and mitochondria seem to be important for

the control of Ca^{2+} entry (Lawrie et al., 1996; Hoth et al., 1997; Montero et al., 2000), and local interactions between adjacent mitochondria allow for the regeneration and spreading of apoptotic signals between mitochondria in some models of apoptosis (Pacher and Hajnóczky, 2001).

Distribution of mitochondria to strategic sites is likely to be established by a cytoskeleton-based transportation system. Mitochondria have been visualized in association with the microfilaments (MFs; Drubin et al., 1993; Morris and Hollenbeck, 1995), microtubules (MTs; Ball and Singer, 1982), and intermediate filaments (Summerhayes et al., 1983; Stromer and Bendayan, 1990) in various cell types. For the binding of cytoskeletal elements, docking proteins have been identified on the mitochondria (e.g., dynactin for the microtubular motor protein, cytoplasmic dynein [Habermann et al., 2001; Varadi et al., 2004], or for both dynein and kinesin [Deacon et al., 2003]). Mitochondria-bound molecular motors provide a means for the organelles to move along the cytoskeletal fibers. Mice lacking Kif1B, the kinesin motor that binds to the mitochondria, are embryonic lethal and in their cells mitochondria are clustered around the nucleus (Tanaka et al., 1998). However, mitochondrial motility is not restricted to the delivery of organelles from the site of biogenesis to their destinations. In fact, mitochondria exist as highly dynamic structures in the cells (for review see Yaffe, 1999). Mitochondrial motility appears in the form of both long-distance travel and complex local movements, mostly wiggling.

Movements may result in a change in the distribution of mitochondria in the cell and, in turn, rearrange the spatial pattern of ATP production and Ca^{2+} buffering. Mitochondrial movements may also increase the chance of dynamic interactions between discrete organelles and may aid the transport of molecules between the cytoplasm and mitochondria. However, movements may interfere with the rapid transport of molecules from an organelle to a neighboring one if the transport depends on activation of the acceptor transport site by a short-lasting concentration surge that is confined to the vicinity of the donor site. A bidirectional coupling has also been proposed between mitochondrial motility and morphology, whereby the dynein–dynactin complex contributes to the mitochondrial targeting of Drp1 that promotes mitochondrial fission to make possible anterograde transport of the mitochondria by kinesin family motors (Varadi et al., 2004). Thus, mitochondrial motility and dynamic changes in motility may affect in many ways the signaling pathways and cell function.

Recently, inhibition of mitochondrial motility was described as an early and Ca^{2+}-dependent event during the NMDA receptor-mediated excitotoxic injury in primary forebrain neurons (Rintoul et al., 2003). Furthermore, evidence has been presented that the direction of movement of mitochondria along the MTs is affected by the level of phosphatidyl inositol 4,5-bisphosphate (De Vos et al., 2003). Cleavage of phosphatidyl inositol 4,5-bisphosphate to produce inositol 1,4,5-trisphosphate (IP_3) and IP_3-induced mobilization of Ca^{2+} to establish $[Ca^{2+}]_c$ oscillations are fundamental steps in the signaling cascade induced by a variety of hormones, neurotransmitters, and growth factors. These observations raise the possibility that mitochondrial motility may be controlled in a dynamic manner by the messenger molecules that mediate the effect of agonists on cell function.

The aims of the present work were to determine how physiological calcium signals affect mitochondrial motility and to study the mechanisms that may relay the effect of calcium to mitochondrial motor proteins. We have established a fluorescence imaging approach to monitor mitochondrial movement activity simultaneously with calcium spikes and oscillations. Using this approach, we show that mitochondrial movement is effectively stopped during both IP_3 receptor– and ryanodine receptor (RyR)–mediated $[Ca^{2+}]_c$ spikes and oscillations in H9c2 myoblasts. Inhibition of motility followed the spatial and temporal pattern of the $[Ca^{2+}]_c$ signal. Although the decay of each $[Ca^{2+}]_c$ spike was followed by recovery of mitochondrial motility, during high frequency $[Ca^{2+}]_c$ oscillations sustained inhibition of mitochondrial motility occurred. Our results also indicate that depression of mitochondrial movement promotes the $[Ca^{2+}]_c$ signal propagation into the mitochondria. Thus, diminished mitochondrial motility in the region of the $[Ca^{2+}]_c$ rise would support recruitment of the mitochondria to enhance local Ca^{2+} buffering and ATP production. The increase in local mitochondrial Ca^{2+} uptake and in the energy supply of Ca^{2+} pumps facilitate the decay of the $[Ca^{2+}]_c$ rise, serving as a feedback mechanism in calcium signaling.

Results

Arrest of mitochondrial movement induced by calcium mobilizing agonists

Rapid motility of the mitochondria was visualized in H9c2 myoblasts expressing enhanced-YFP targeted to the mitochondrial matrix via a fusion with the targeting sequence of cytochrome *c* oxidase subunit VIII (mitoYFP; Video 1, available at http://www.jcb.org/cgi/content/full/jcb.200406038/DC1). Mitochondria exhibited both short- and long-range movements. Strikingly, when vasopressin (VP), a Ca^{2+} mobilizing hormone, was added to the cells, mitochondria were promptly stopped and subsequently gradually regained motility (Video 1). Similar to the mitoYFP-expressing cells, the vigorous mitochondrial movement and inhibition of motility by VP was also observed in mitoDsRed-expressing or in Mitotracker green–loaded cells (unpublished data).

As a first approach to evaluate the mitochondrial motility, two images obtained 10 s apart from each other were colored green and red, respectively, and were subsequently overlaid (Fig. 1 A, i). In the overlay, the yellow (green+red) pixels represent the mitochondria that maintained their position, whereas the green and red pixels indicate the sites of movement. One way to show only the sites of movement is to calculate the difference of the two images ($F_{-13.3s} - F_{-23.2s}$; Fig. 1 A, ii, negative values shown in green, positive values in red, respectively). The amount and distribution of green and red pixels in the difference image corresponds with that in the overlay image (Fig. 1 A, i and ii). Green and red pixels are mostly side-by-side, indicating lateral movement of the organelles, whereas the single green or red pixels are likely to reflect movement into or out of the focus plane. Similar analysis was performed with two images recorded after addition of VP. In this case, very few green and red pixels were obtained, confirming a decrease in mitochondrial mobility (Fig. 1 A, iii and iv).

To show the time course of the VP-induced decrease in mitochondrial motility, the difference image protocol was extended. By subtraction of sequential images (3.3-s interval), the fluorescence change for each pixel was calculated, and pixels that exhibited a change (positive or negative) greater than a threshold were counted for each time point. Changes in the pixel number were normalized to the initial value calculated for cells before stimulation. As shown in Fig. 1 A (v), the number of pixels with a fluorescence change exhibited a sharp decrease when the stimulation with VP started and subsequently showed a gradual increase. To test the effect of VP on slow directional movements, we have also calculated difference images using 40 s interval and counted the >3 μm shifts. In the prestimulation period, 8.3 ± 2.7 events per cell were counted, whereas during both the VP-induced calcium spike (0 to 40 s of the stimulation) and the gradual decay phase of the calcium signal (40 to 80 s of the stimulation) 0 events per cell were counted ($n = 3$). These data suggest that both the directional movement and the wiggling of the mitochondria were essentially eliminated immediately after addition of VP and then, gradually, partially recovered.
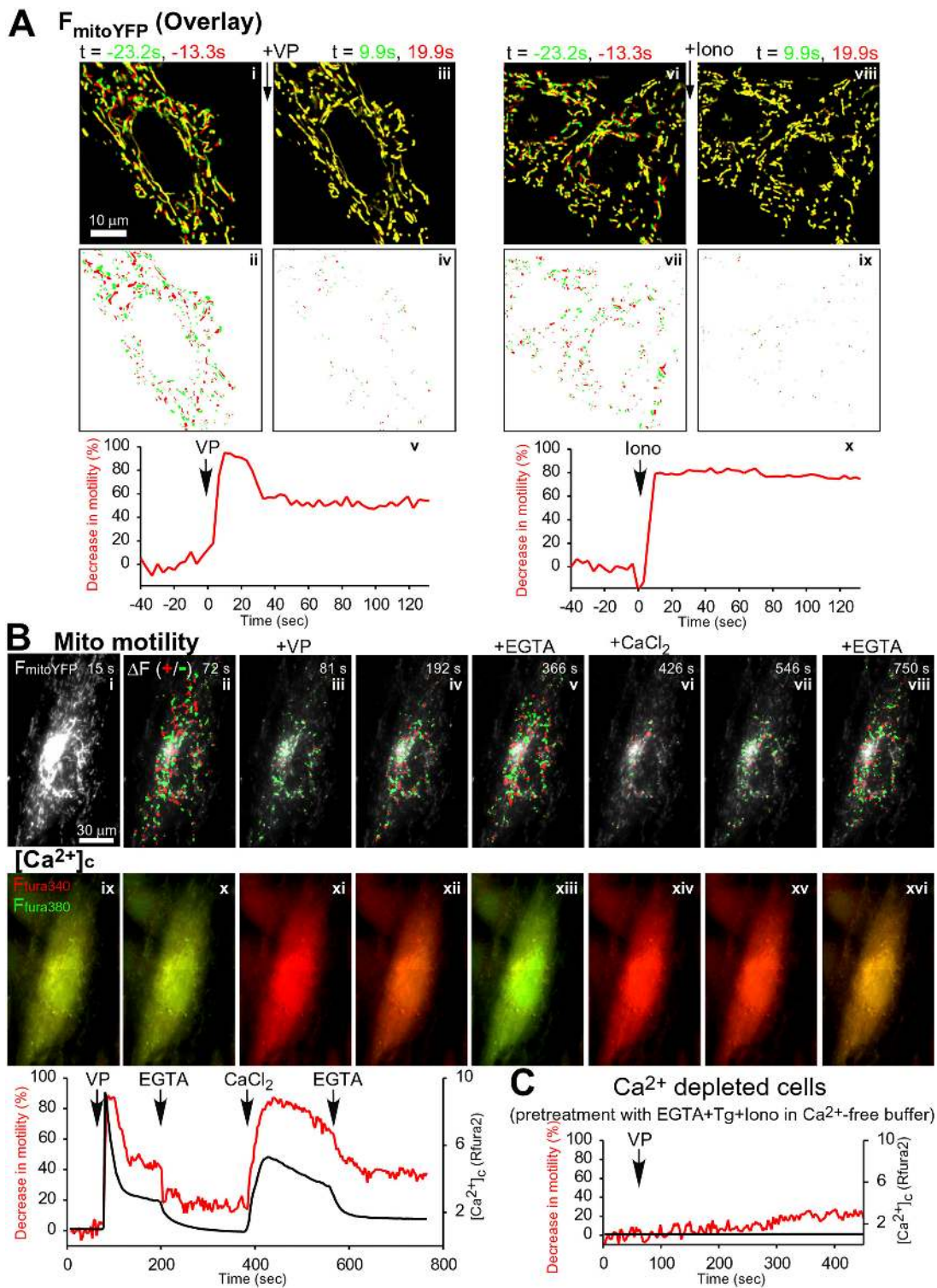
Figure 1. **Stimulus-induced inhibition of mitochondrial motility.** (A) Measurement of mitochondrial movement in H9c2 cells. Green/red overlay of two time-lapse confocal images ($\Delta t = 10$ s) of mitoYFP fluorescence in a live cell before (i) and after (iii) stimulation by 100 nM VP. (ii and iv) Processed images showing only the pixels whose values differ by more than a threshold value (+ and −) between the two time points. (v) Graph of the number of pixels that change more than the threshold value for this cell, calculated with consecutive images ($\Delta t = 3.3$ s), and normalized as the percentage of loss from the average before stimulation. (vi–x) Two cells stimulated by addition of 10 μM Iono. Graph shown is the mean of the two cells. (B) Simultaneous measurements of mitochondrial motility and $[Ca^{2+}]_c$ in an H9c2 cell expressing mitoYFP and loaded with fura2. Top row of images shows both mitoYFP fluorescence (grayscale; i scaled with higher contrast to show the structure of the mitochondria) and at each time point, the sites of mitochondrial movement calculated by subtraction of sequential images (red, positive changes; green, negative changes). Bottom row of images shows fura2 fluorescence measured using excitation of both the Ca^{2+}-bound (340 nm, red) and the Ca^{2+}-free form (380 nm; green). Thus, $[Ca^{2+}]_c$ elevations evoked by addition of VP (81 s) and $CaCl_2$ (426 s) appear as an increase in the red component. In the histogram, the decrease in mitochondrial motility (calculated as in A) and $[Ca^{2+}]_c$ (ratio of the fluorescence of the Ca^{2+} bound and Ca^{2+}-free forms of fura2) are plotted in red and black, respectively. The cell was treated sequentially with 100 nM VP, 5 mM EGTA, 10 mM $CaCl_2$, and 5 mM EGTA. (C) Lack of change in mitochondrial motility in the absence of the VP-induced $[Ca^{2+}]_c$ rise. The cell was preincubated with 2 mM EGTA, 2 μM Tg, and 10 μM Iono in Ca^{2+}-free ECM to remove extracellular Ca^{2+} and to deplete the intracellular Ca^{2+} stores before stimulation with 100 nM VP. Mitochondrial motility and $[Ca^{2+}]_c$ are plotted as in B.

Figure 2. **Relationship between $[Ca^{2+}]_c$ and mitochondrial motility.** (A) Stepwise increases in $[Ca^{2+}]_c$ induce stepped decreases in mitochondrial motility. MitoYFP-expressing and fura2-loaded cells were incubated in Ca^{2+}-free ECM supplemented with 2 mM EGTA, 2 μM Tg, and 10 μM of Iono for 12 min. Simultaneous measurements of $[Ca^{2+}]_c$ and mitochondrial motility were performed in single cells exposed to stepped increases in extracellular $CaCl_2$ from 0 to 15 mM. $[Ca^{2+}]_c$ was calibrated in terms of nanomoles using in vitro calibration of fura2. (B) Dose–response relationship between $[Ca^{2+}]_c$ and mitochondrial motility. Simultaneous measurements of $[Ca^{2+}]_c$ and mitochondrial motility were performed in single cells as described for A. Mean mitochondrial motility inhibition and mean $[Ca^{2+}]_c$ were calculated for each $[CaCl_2]$. Mean ± SEM are marked by filled circles ($n = 68$ cells from 40 experiments). The $IC_{50} \approx 400$ nM, indicating that mitochondrial motility is controlled in the physiological range of $[Ca^{2+}]_c$. (C) Mitochondrial motility (red line) and $[Ca^{2+}]_c$ (black line) were recorded in single cells stimulated by varying doses of VP (0.1–100 nM). In addition, the mean mitochondrial motility inhibition and mean $[Ca^{2+}]_c$ were calculated for each VP concentration and are plotted in B (empty circles and dashed line; $n = 44$ cells from 28 experiments).
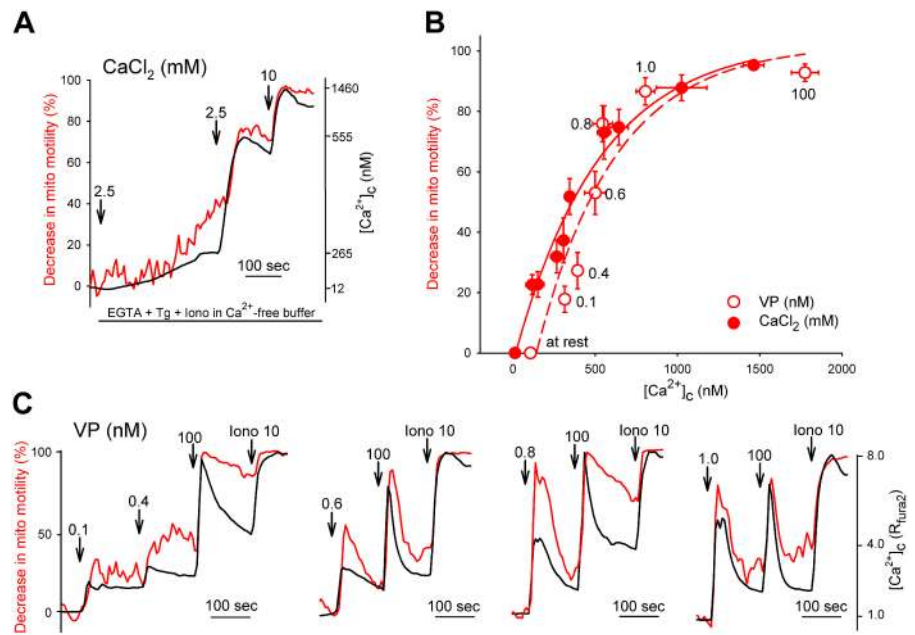
A fundamental second messenger mobilized by VP is Ca^{2+} that controls many forms of motility. To test the possibility that the Ca^{2+} signal was important for the VP effect on mitochondrial motility, cells were also treated with ionomycin (Iono), a Ca^{2+} ionophore that allows both Ca^{2+} release from intracellular stores and Ca^{2+} entry from the bathing medium to elevate $[Ca^{2+}]_c$. Iono triggered a rapid and almost complete loss of motility (Fig. 1 A, v–x). Thus, a rise in $[Ca^{2+}]$ is likely to account for the arrest of mitochondrial movement.

To determine the relation between the $[Ca^{2+}]_c$ signal and mitochondrial motility, cells expressing mitoYFP were loaded with fura2/AM, a Ca^{2+}-sensitive fluorescent probe, and $[Ca^{2+}]_c$ was monitored simultaneously with YFP fluorescence. As shown in Fig. 1 B, the VP-induced decrease in mitochondrial motility (Fig. 1 B, top row) was closely coupled to the rising phase of the $[Ca^{2+}]_c$ spike (Fig. 1 B, bottom row) and the recovery of mitochondrial motility lagged slightly behind the decay of the $[Ca^{2+}]_c$ signal. During the $[Ca^{2+}]_c$ signal, removal of extracellular Ca^{2+} by EGTA caused $[Ca^{2+}]_c$ to return to the resting level and at the same time, mitochondrial motility to return to the original activity (Fig. 1 B). When Ca^{2+} was added back to the bathing medium, Ca^{2+} entry provided for a substantial $[Ca^{2+}]_c$ increase. This $[Ca^{2+}]_c$ signal was also closely followed by inhibition of mitochondrial movement. Again, the $[Ca^{2+}]_c$ rise and the inhibition could be reversed by addition of EGTA (Fig. 1 B). To ascertain the role of Ca^{2+} in the effect of VP, VP was also added to Ca^{2+}-depleted cells. In the absence of a $[Ca^{2+}]_c$ rise, no VP-induced change in mitochondrial movement was recorded (Fig. 1 C). Together, these results show that the mitochondrial motility is dynamically controlled by the VP-induced, IP_3-linked $[Ca^{2+}]_c$ signal.

Control of mitochondrial motility in the physiological range of global $[Ca^{2+}]_c$

When EGTA and Iono were added together to nonstimulated cells to lower the $[Ca^{2+}]_c$ no change in mitochondrial movement activity was observed ($n = 4$; unpublished data), suggesting that the motility was maximal at the resting level of $[Ca^{2+}]_c$ (50–100 nM). To quantitate the $[Ca^{2+}]_c$ dependence of the inhibition of mitochondrial motility, $[Ca^{2+}]_c$ and motility were measured in cells that were incubated in a Ca^{2+} free buffer supplemented with EGTA, thapsigargin (Tg), an inhibitor of the sarco-endoplasmic reticulum Ca^{2+} pump and Iono to ensure rapid equilibration of the cytosol with the extracellular $[Ca^{2+}]$, and then varying amounts of $CaCl_2$ were added (Fig. 2, A and B). As shown in Fig. 2 A, stepwise increases in $[Ca^{2+}]_c$ were accompanied with stepwise decreases in mitochondrial motility. The inhibition of motility was plotted against the $[Ca^{2+}]_c$ (Fig. 2 B, filled circles). The majority of the Ca^{2+}-induced attenuation of mitochondrial motility was obtained in the sub-micromolar range of $[Ca^{2+}]_c$ ($IC_{50} \approx 400$ nM), indicating that mitochondrial motility is controlled in the physiological range of $[Ca^{2+}]_c$.

In VP-stimulated cells, the inhibition of mitochondrial motility was also in proportion to the agonist dose and the size of the $[Ca^{2+}]_c$ elevation (Fig. 2 C). Low doses of VP (e.g., 0.1 nM) were sufficient to cause considerable inhibition of the movement (Fig. 2 C). When the VP-induced inhibition of motility was plotted against the VP-induced $[Ca^{2+}]_c$ rise, the data points were close to the curve obtained by the in situ $[Ca^{2+}]_c$ titration (Fig. 2 B, filled circles). In other words, the competence of VP to attenuate mitochondrial movement was in proportion to the $[Ca^{2+}]_c$ signal. Thus, inhibition of mitochondrial movement during IP_3-mediated Ca^{2+} mobilization can be attributed to the $[Ca^{2+}]_c$ signal.
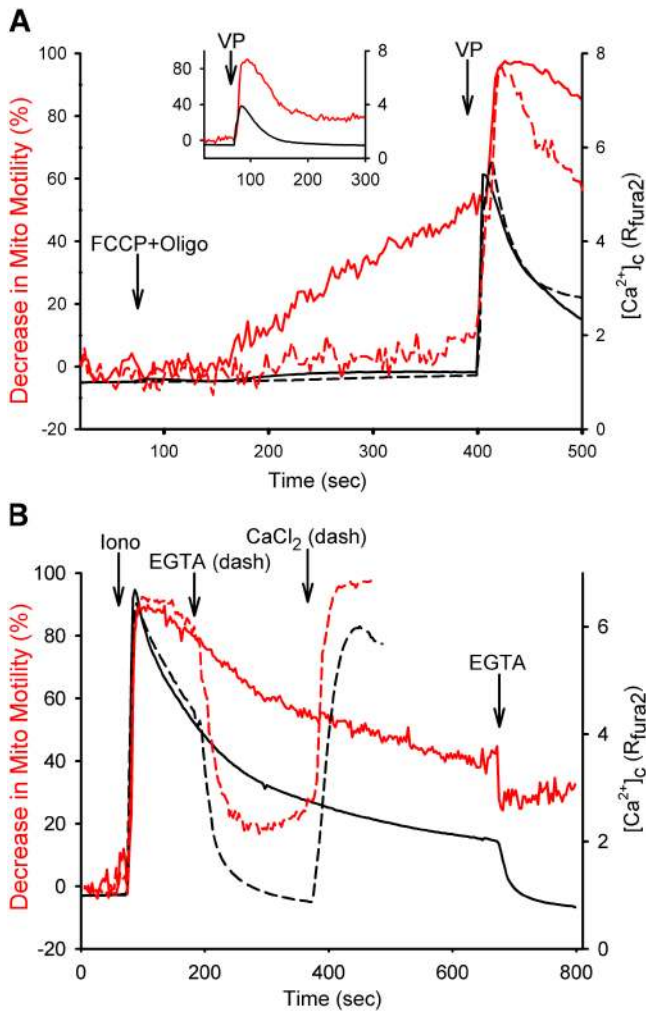
Figure 3. **Spatio-temporal pattern of the calcium signal and inhibition of mitochondrial motility.** (A) Calcium signal propagation to the mitochondria is not required for the inhibition of motility. Uncoupler (5 μM FCCP and 5 μg/ml Oligo; solid line) or solvent (dashed line) was added to the cells 5 min before stimulation with VP. The uncoupler causes dissipation of the $\Delta\Psi_m$ in <1 min and in turn decreases the driving force of the mitochondrial Ca^{2+} uptake in H9c2 myoblasts (Szalai et al., 2000). Mitochondrial motility showed a slowly developing decrease (red solid line) compared with the control (red dash line). However uncoupler did not prevent the effect of VP on mitochondrial motility, indicating that mitochondrial Ca^{2+} uptake and $\Delta\Psi_m$ were not necessary for the control of motility by the calcium signal. In another set of experiments, the cells were pretreated with uncoupler for 10 min before the recording was started. The inset shows that the residual motility was effectively inhibited by 100 nM VP. Data are the means of nine experiments with uncoupler and four experiments for the control. (B) Reversible and reproducible inhibition of mitochondrial motility by Ca^{2+}. To evaluate the effect of pulsatile increases of $[Ca^{2+}]_c$ (black traces) on mitochondrial motility (red traces), the 10 μM of Iono-induced $[Ca^{2+}]_c$ elevation was recorded for 10 min (solid lines) or was reversed by addition of 5 mM EGTA and, subsequently, was reestablished by addition of 10 mM $CaCl_2$ (dashed lines). Data are the means of 36 cells from 22 experiments.

## No role for mitochondrial Ca²⁺ uptake and mitochondrial membrane potential (ΔΨₘ) in the arrest of mitochondrial motility by Ca²⁺

The IP$_3$-induced $[Ca^{2+}]_c$ signal is propagated to the mitochondria, giving rise to a mitochondrial matrix $[Ca^{2+}]$ ($[Ca^{2+}]_m$) rise that controls the activity of Ca^{2+}-dependent enzymes and ion

channels (for review see Duchen, 2000). The primary driving force of the mitochondrial Ca^{2+} uptake is the $\Delta\Psi_m$ that also drives mitochondrial ATP synthesis. To determine whether the $[Ca^{2+}]_m$ signal or $\Delta\Psi_m$ is necessary for the Ca^{2+}-dependent inhibition of mitochondrial motility, we treated cells with an uncoupler (FCCP added with the ATPase inhibitor, oligomycin to preserve cytosolic ATP; Fig. 3 A). This treatment has been shown to cause rapid dissipation of the $\Delta\Psi_m$ (Pacher and Hajnóczky, 2001) and to reduce mitochondrial Ca^{2+} uptake in H9c2 cells (Szalai et al., 2000). Uncoupler induced a slow attenuation in mitochondrial motility (Fig. 3 A), which may reflect a fall in perimitochondrial ATP that is likely to be needed for movement. However, the VP-induced arrest of mitochondrial movement was preserved in uncoupler-pretreated cells (Fig. 3 A). Thus the $[Ca^{2+}]_m$ signal and $\Delta\Psi_m$ appears to be dispensable for the Ca^{2+}-mediated inhibition of mitochondrial movement.

Spatio-temporal control of the mitochondrial movement by [Ca²⁺]ᴄ oscillations and waves

Our data have shown that the control of mitochondrial motility can respond to repetitive stimulation by an IP$_3$-linked agonist (Fig. 2 C). Along this line, Fig. 3 B shows that the $[Ca^{2+}]_c$ rise-induced inhibition of mitochondrial movement can be reversed by termination of the $[Ca^{2+}]_c$ elevation and subsequently, reproduced by a second step of $[Ca^{2+}]_c$ elevation. This suggests that no desensitization of the Ca^{2+} regulation of mitochondrial motility occurred. If there is no desensitization and the reversal of the movement inhibition is slower than the decay of the $[Ca^{2+}]_c$ spike, $[Ca^{2+}]_c$ oscillations may be able to cause a prolonged depression of mitochondrial motility. In differentiated H9c2 myotubes, RyR-mediated $[Ca^{2+}]_c$ oscillations have been demonstrated (Szalai et al., 2000). As shown in Fig. 4, $[Ca^{2+}]_c$ oscillations were also observed in H9c2 myoblasts transfected with RyR1 (Bhat et al., 1997) and stimulated with caffeine (Caff). Similar to the IP$_3$-linked $[Ca^{2+}]_c$ spikes, the RyR-mediated $[Ca^{2+}]_c$ spikes also triggered inhibition of mitochondrial motility and the oscillations of $[Ca^{2+}]_c$ were often associated with oscillations in movement activity (Fig. 4 A, cell marked by an arrow). Each burst of RyR1-mediated Ca^{2+} release could result in maximal inhibition of mitochondrial motility (Fig. 4, A and B). Isolated spikes of mitochondrial movement inhibition were observed during low frequency $[Ca^{2+}]_c$ oscillations (unpublished data). However, if the frequency of $[Ca^{2+}]_c$ spiking was higher and the recovery of motility was slow, $[Ca^{2+}]_c$ oscillations could produce an essentially sustained maximal inhibition in movement activity (Fig. 4 B). Thus the frequency-modulated $[Ca^{2+}]_c$ signals are translated into a time-averaged motility response. Notably, at supramaximal stimulation the $[Ca^{2+}]_c$ oscillations run together and fuse into a large and slowly decaying single $[Ca^{2+}]_c$ spike (Szalai et al., 2000), but this $[Ca^{2+}]_c$ signal could not provide for sustained inhibition of the mitochondrial motility (e.g., Fig. 1 B). In this way, the control of mitochondrial motility may serve as a model whereby $[Ca^{2+}]_c$ oscillations are an effective signal for long-term modulation, but a nonoscillatory $[Ca^{2+}]_c$ signal is unable to maintain inhibition.
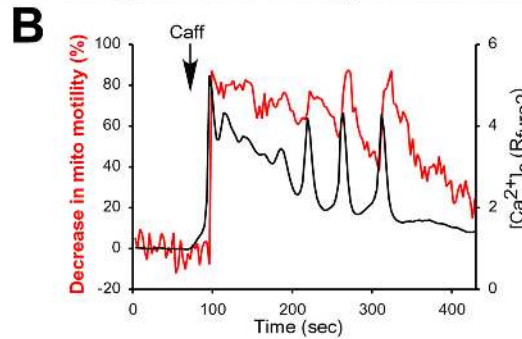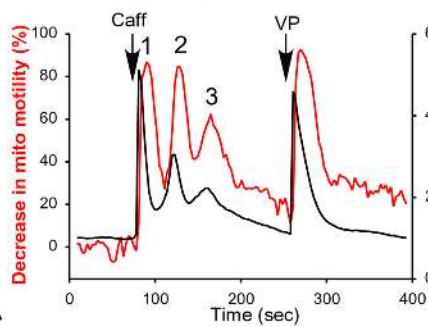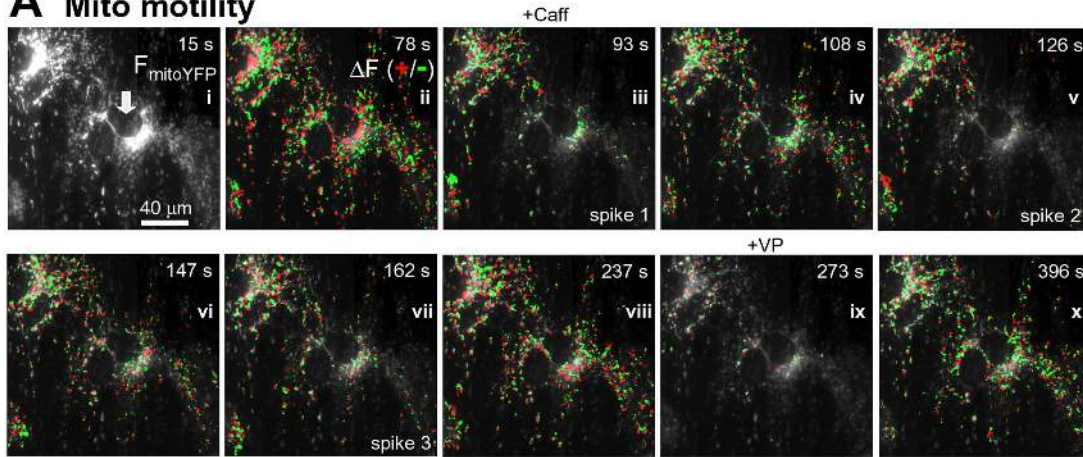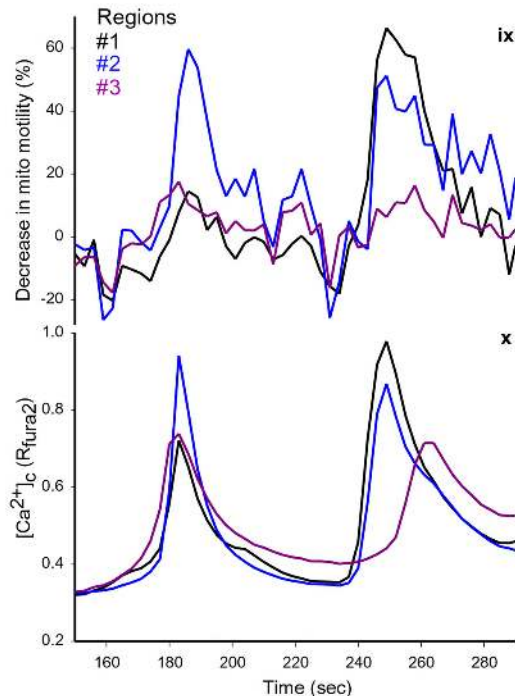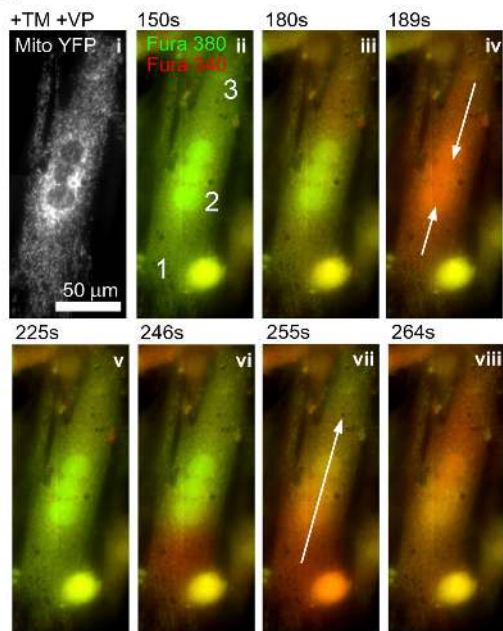
Figure 4. **Control of mitochondrial motility by [Ca²⁺]$_c$ oscillations and waves.** Mitochondrial motility was evaluated simultaneously with [Ca²⁺]$_c$ in cells cotransfected with constructs encoding mitoYFP and RyR1 and loaded with fura2. To promote RyR-mediated Ca²⁺ mobilization, the cells were exposed to 10 mM of caffeine (Caff). (A) In the image series, mitochondrial movements are visualized in a cell that showed [Ca²⁺]$_c$ oscillations in response to stimulation by Caff (arrow) and in a cell that did not show a Caff-induced [Ca²⁺]$_c$ rise (top left corner) as described for Fig. 1. Also shown is the effect of 100 nM VP that elicited a [Ca²⁺]$_c$ signal in both cells. The time course of [Ca²⁺]$_c$ (black trace) and mitochondrial motility (red trace) for the Caff-sensitive cell is plotted. (B) Sustained inhibition of mitochondrial motility in a cell that displayed a relatively high frequency [Ca²⁺]$_c$ oscillation in response to stimulation by Caff. (C) Calcium waves were induced in mitoYFP-expressing cells by treatment with 75 μM thimerosal (TM) and 0.1 nM VP. The image series shows the mitoYFP fluorescence (i) and the first two calcium waves after addition of VP and TM (t = 60 s; ii–ix). The first wave begins simultaneously at the ends of the cell and converges in the center as indicated by the arrows (iv). The second wave begins at the lower end of the cell and weakens as it propagates to the top (vi–viii, arrow marks the direction of the wave propagation in vii). Measurement of [Ca²⁺]$_c$ (x) and mitochondrial movement (ix) in three distinct regions of the cell, labeled 1–3 in panel ii, reveals spatio-temporal heterogeneity in the inhibition of movement corresponding to the local calcium concentration.
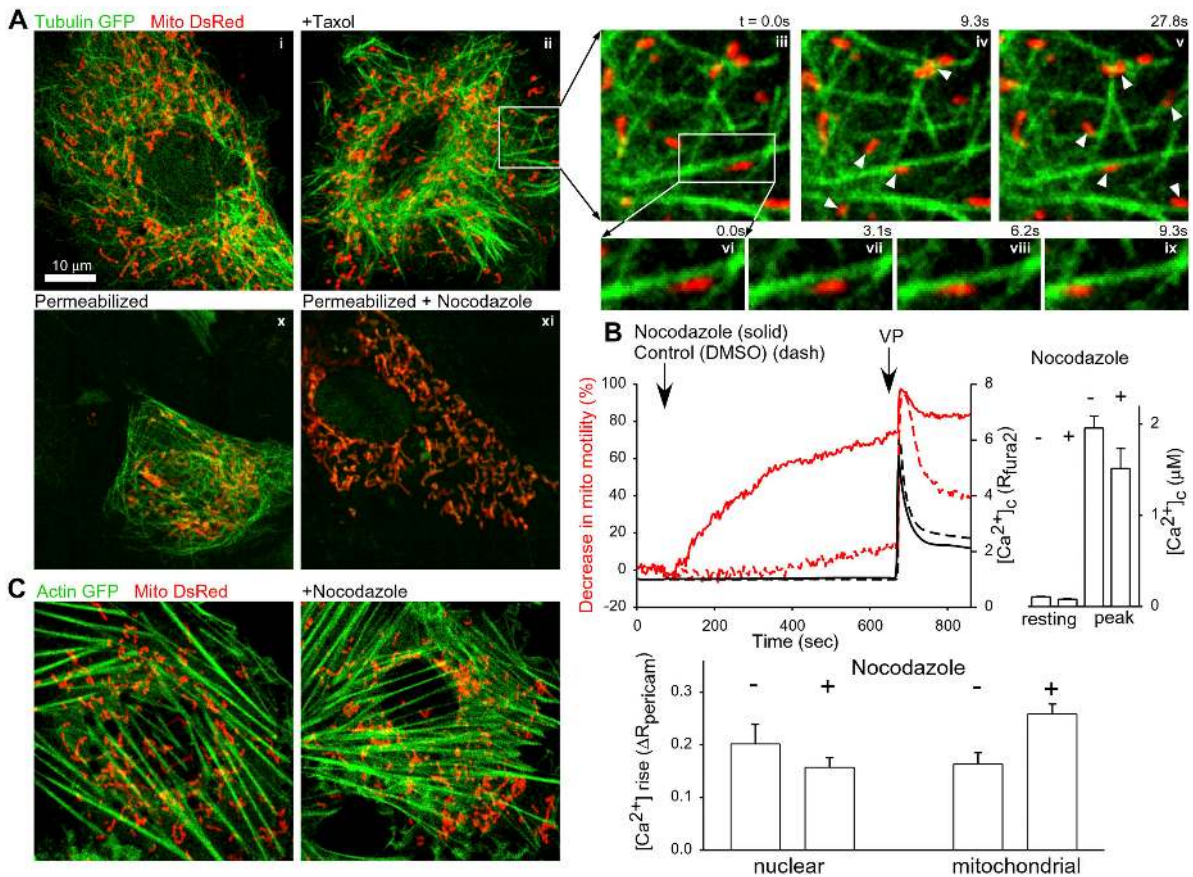
Figure 5. **Spatial relationship between MTs, MFs, and mitochondria.** (A) H9c2 cells expressing tubulinGFP and mitoDsRed and incubated in the absence (i) or presence (ii) of 10 μM of an MT-stabilizing agent, taxol. (iii–v) Magnified time-lapse images of a peripheral region of the taxol-pretreated cell. Arrowheads mark the mitochondria that move substantially from the previous image. (vi–ix) Further magnified region showing a single mitochondrion sliding along an MT. (x and xi) A naive and a nocodazole-pretreated cell after permeabilization with digitonin. (B) Inhibition of mitochondrial motility and enhancement of the VP-induced mitochondrial [Ca^{2+}] signal in nocodazole-pretreated cells. (top left) Mitochondrial motility and [Ca^{2+}]$_c$ in nocodazole-treated cells (solid lines, 23 cells in 10 measurements) as compared with control cells (dashed lines, 22 cells in 11 measurements). The effect of 100 nM VP is also shown. (top right) Resting [Ca^{2+}]$_c$ and the peak value of the VP-induced [Ca^{2+}]$_c$ signal in control and nocodazole-pretreated (10 μM for 25–30 min) cells. (bottom) Nuclear matrix and mitochondrial matrix [Ca^{2+}] measured in cells expressing both nuclear and mitochondrial pericam using fast, ratiometric imaging (2 ratio/s). Cells were pretreated with nocodazole (10 μM for 25–30 min) or solvent (control) and stimulated by 100 nM VP. The VP-induced initial [Ca^{2+}]$_c$ signal was measured (change in nuclear pericam fluorescent ratio at the first point of the [Ca^{2+}] rise, <25% of the maximal change) and the corresponding change in [Ca^{2+}]$_m$ (change in mitochondrial pericam fluorescent ratio) was calculated for each cell (mean ± SEM; n = 16). (C) MFs and mitochondria in H9c2 cells expressing actinGFP and mitoDsRed. Cells were incubated in the absence or presence of 10 μM of nocodazole.

The [Ca^{2+}]$_c$ signal often displays regional heterogeneity that may also result in heterogeneity in the mitochondrial motility. To test this possibility, we studied mitochondrial motility in cells that showed spatial heterogeneity in the [Ca^{2+}]$_c$ rise. In the cell shown in Fig. 4 C, the first [Ca^{2+}]$_c$ wave started simultaneously at the ends of the cell (regions 1 and 3) and converged in the center (region 2) as indicated by the arrows (iv). The [Ca^{2+}]$_c$ rise was relatively large in the center (Fig. 4 C, x). Reproducing the spatial pattern of the [Ca^{2+}]$_c$ signal, inhibition of the mitochondrial motility was substantially larger in the center than at the ends of the cell (Fig. 4 C, ix). The second [Ca^{2+}]$_c$ wave began at the lower end of the cell and weakened as it propagated to the top (Fig. 4 C, vi–viii). Similarly, the inhibition of mitochondrial motility was substantial at the lower end, smaller in the center, and hardly noticeable at the upper end (Fig. 4 B, ix). This experiment revealed intracellular spatio-temporal heterogeneity in the inhibition of movement corresponding to the local

[Ca^{2+}]$_c$ concentration. Such differences in the movement may affect the spatial distribution of mitochondria. Mitochondria would be stopped in the vicinity of the active Ca^{2+} release sites. If mitochondria stay in high [Ca^{2+}]$_c$ areas for a relatively long time and cross quickly through low [Ca^{2+}]$_c$ areas, this also provides a mechanism for the redistribution of mitochondria to the regions of high [Ca^{2+}]$_c$. Notably, one or two localized [Ca^{2+}]$_c$ spikes did not result in an obvious increase in the mitochondrial density (unpublished data). Acquisition of mitochondria from low [Ca^{2+}]$_c$ zones may require prolonged or repetitive Ca^{2+} release because it would not be driven by an attractive force but would use immobilization of mitochondria that move into the region of the [Ca^{2+}]$_c$ rise on their own. However, stabilization of the position of the mitochondria in the areas of Ca^{2+} release seems to be sufficient to promote the delivery of [Ca^{2+}]$_c$ spikes to the mitochondria (see Arrest of the mitochondria supports rapid Ca^{2+} delivery to the mitochondria). Thus, through the control

of motility, the spatial distribution of the mitochondrial Ca^{2+} buffering and ATP production may be dynamically regulated by the local $[Ca^{2+}]_c$.

Organization of mitochondrial motility by the MTs

Long-range mitochondrial movements are facilitated by the MTs and certain forms of local movement may use the MFs (Couchman and Rees, 1982; Nangaku et al., 1994; Morris and Hollenbeck, 1995; Varadi et al., 2004). In H9c2 myoblasts expressing tubulinGFP and DsRed targeted to the mitochondria, green fluorescence both marked a complex network of fibers and appeared as a homogeneous signal throughout the cells (Fig. 5 A, i). Labeling of the fibers became more intense, and the homogeneous signal effectively disappeared when the cells were pretreated with taxol, a drug that promotes the polymerization of tubulin (Fig. 5 A, ii). The fibers were retained and the homogeneous signal was promptly eliminated if the cells were permeabilized (Fig. 5 A, x). Based on these data, the fibers represent the MTs and the homogeneous fluorescence is likely to be accounted by monomeric tubulinGFP.

Distribution of the red fluorescence showed colinearity of the long axis of tubular mitochondria and MTs (Fig. 5 A, i–iii and x; Video 2, available at http://www.jcb.org/cgi/content/full/jcb.200406038/DC1). Furthermore, the time series of images shows that mitochondria move along MTs (Fig. 5 A, iii–v, arrows point to the sites of movement). Similar to the mitochondrial movement shown in a taxol-pretreated cell (Fig. 5 A, vi–ix), in control cells, the average rate was 0.31 ± 0.05 µm/s ($n = 19$) for mitochondria that showed continuous movement along a straight track for ≥ 10 s. The dynamics of mitochondrial motility along the MTs is further illustrated by a movie sequence (Video 2). To quantify the MT-associated movement, for each mitochondrion that moved ≥ 3.5 µm, it was evaluated whether or not the movement was along an MT. In four cells, 49 out of 68 mitochondria (72%) followed the track of MTs and no mitochondrion (0%) moved clearly independent of the MTs. For the remaining 17 mitochondria (28%), it was not possible to discern if the movement was along an MT, due to the homogeneous tubulinGFP fluorescence in some regions of the cells. Exposure of the cells to nocodazole (10 µM), a drug disrupting the tubulin polymers resulted in loss of the MTs without inducing a major change in mitochondrial morphology (Fig. 5 A, x and xi). However, mitochondrial motility displayed a progressive decrease in nocodazole-treated cells (Fig. 5 B). Strikingly, the nocodazole-induced inhibition of mitochondrial motility occurred in the absence of a $[Ca^{2+}]_c$ elevation (Fig. 5 B). However, nocodazole evoked a decrease in ER Ca^{2+} storage because the VP-induced Ca^{2+} mobilization was smaller in nocodazole-pretreated cells (Fig. 5 B, histograms).

In cells expressing actinGFP and mitoDsRed, the green fluorescence showed fibers (Fig. 5 C, left) that were also labeled with rhodamine-phalloidin, an MF-specific tracer ($n = 4$; not depicted). Although the red fluorescent mitochondria often appeared close to the MFs, usually mitochondria were not aligned to the MFs (Fig. 5 C, left). In the time series of images, the movement of the mitochondria along the MFs was quantified as described for the movement along the MTs above. In four cells, only 10 out of 66 mitochondria (15%) followed the track of an MF, whereas 37 mitochondria (56%) appeared to move independent of the MFs. In the remaining 19 cases (29%), it was not possible to discern whether or not the movement was along an MF. In regard to the role of MFs in mitochondrial motility it is also relevant that the MFs were undamaged in nocodazole-treated cells (Fig. 5 B, right), which did not display considerable mitochondrial movement activity (Fig. 5 B). Collectively, the aforementioned data suggest that mitochondrial movement depends on the integrity of the MTs and closely follows the tracks provided by the MTs. Furthermore, MFs alone do not appear to provide the primary track for mitochondrial movements.

In the movement of mitochondria along MTs, cytoplasmic dynein and kinesin (Kif1b)-based motors are likely to play a role. Mitochondrion-specific kinesin heavy and light chains have been identified in mammalian cells (Nangaku et al., 1994; Khodjakov et al., 1998). However, recent resolution of the molecular structure of the mammalian cytoplasmic dynein and kinesin did not reveal any Ca^{2+} or CaM binding site (for review see Vale, 2003). Furthermore, we have observed that neither inhibitors of the Ca^{2+}/CaM-dependent kinases (KN-62, 10 µM, $n = 5$; KN-93, 5 µM, 30 min pretreatment, $n = 5$; myristoylated-autocamtide-2–related inhibitory peptide, 10 µM, 1 h pretreatment, $n = 5$) nor inhibitors of calcineurin, the Ca^{2+}-dependent protein phosphatase (cyclosporine A, 5 µM, $n = 3$; FK506 10 µM, 30 min, $n = 5$; deltamethrin 10 µM, 30 min pretreatment, $n = 5$) prevented the VP-induced inhibition of mitochondrial motility. Based on these data, the Ca^{2+} signal is not likely to control mitochondrial movement through phosphorylation or dephosphorylation of dynein or kinesin. Thus, it seems that a distinct Ca^{2+} sensor molecule is required to translate the Ca^{2+} signal for the microtubular motor proteins.

Arrest of the mitochondria supports rapid Ca^{2+} delivery to the mitochondria

Movement is important for the delivery of mitochondria from the site of biogenesis to the sites where energy is needed. Furthermore, the present data on the spatio-temporal control of the movement by the $[Ca^{2+}]_c$ signal shows immobilization of mitochondria in the regions that display a $[Ca^{2+}]_c$ rise (Fig. 4 C). Because mitochondria have the capacity to accumulate Ca^{2+}, another role of the movement and Ca^{2+}-induced inhibition of the movement may be to dynamically control the distribution of the mitochondrial Ca^{2+} buffer to the spatial pattern of the ER/SR Ca^{2+} release or Ca^{2+} entry. In many paradigms, Ca^{2+} signal propagation to the mitochondria depends on exposure of the mitochondrial Ca^{2+} uptake sites to the high $[Ca^{2+}]$ microdomains generated in the vicinity of the ER/SR Ca^{2+} release sites (Rizzuto et al., 1993; 1998; Szalai et al., 2000; Pacher et al., 2002; for comparison see Collins et al., 2001). Movement may affect the distance between ER/SR and mitochondria and may affect the alignment between the Ca^{2+} release and uptake sites if there is physical coupling between the two organelles.

We postulated that rapid inhibition of the mitochondrial movement may promote the mitochondrial Ca^{2+} uptake during

the brief Ca²⁺ release events. We first sought for a means to prevent the inhibition of mitochondrial movement by the calcium signal and to study $[Ca^{2+}]_m$ in mitochondria that are not arrested by the $[Ca^{2+}]_c$ signal. However, no approach has been identified to uncouple the inhibition of mitochondrial movement from the $[Ca^{2+}]_c$ rise. Therefore, we tried to use the $[Ca^{2+}]_c$-independent decrease in mitochondrial movement induced by nocodazole (Fig. 5 B). Because the arrest of mitochondrial movement appears after the onset of the $[Ca^{2+}]_c$ signal, we speculated that inhibition of mitochondrial motility by nocodazole-pretreatment may enhance the initial phase of the $[Ca^{2+}]_m$ signal. To test this idea, cells were transfected with two constructs encoding ratiometric pericam, a Ca²⁺-sensitive fluorescent protein targeted to the nucleus and mitochondria, respectively (Nagai et al., 2001). Before stimulation, the cells were pretreated with nocodazole (10 μM for 20–30 min) or with solvent (DMSO) and were stimulated with VP, while ratiometric imaging of pericam fluorescence was performed. By measuring separately the extranuclear and nuclear areas, $[Ca^{2+}]_m$ was determined simultaneously with nuclear matrix $[Ca^{2+}]$. Nuclear matrix $[Ca^{2+}]$ was used as a surrogate of $[Ca^{2+}]_c$ that was not feasible to monitor simultaneously with $[Ca^{2+}]_m$. In separate experiments, no difference was noticed between the kinetics of the $[Ca^{2+}]$ signals recorded in VP-stimulated cells by cytosolic and nuclear pericam, respectively ($n = 4$; unpublished data).

The initial nuclear $[Ca^{2+}]$ rise was determined for both control and nocodazole-pretreated cells and the simultaneously measured $[Ca^{2+}]_m$ rise response was also evaluated for the same cells (Fig. 5 B, bottom). The nuclear $[Ca^{2+}]$ rise was smaller in the nocodazole-pretreated cells than in the control cells. In contrast, the $[Ca^{2+}]_m$ elevation was >60% greater in the nocodazole-pretreated cells than in the control cells ($P < 0.01$; $n = 16$). Thus, at the beginning of Ca²⁺ mobilization, the efficacy of the $[Ca^{2+}]_c$ signal delivery to the mitochondria was increased in nocodazole-pretreated cells. Although it remains to find a more specific inhibitor of the mitochondrial motility, our result seems to support the idea that the arrest of mitochondrial motility during the $[Ca^{2+}]_c$ signal promotes the $[Ca^{2+}]_c$ signal propagation to the mitochondria. During repetitive stimulation or during $[Ca^{2+}]_c$ oscillations (Fig. 5), the movement inhibition evoked by the first $[Ca^{2+}]_c$ spike may last until the second $[Ca^{2+}]_c$ spike rises and may facilitate the effect of the second $[Ca^{2+}]_c$ spike on the mitochondria. Thus, inhibition of motility may provide a mechanism underlying the enhancement of mitochondrial calcium signaling during $[Ca^{2+}]_c$ oscillations, a phenomenon that has been documented in several paradigms (for review see Csordás and Hajnóczky, 2003). The effective propagation to the mitochondria enables frequency-modulated $[Ca^{2+}]_c$ oscillations to control the Ca²⁺-sensitive enzymes of ATP production over the full range of potential activities (Hajnóczky et al., 1995; Robb-Gaspers et al., 1998).

Discussion

The present work described for the first time the control of mitochondrial motility by the calcium signal and has provided evidence that the Ca²⁺-induced inhibition of mitochondrial motility may be important for optimal delivery of the calcium signal to the mitochondria. We have shown that physiological $[Ca^{2+}]_c$ can control mitochondrial movement over the full range of potential activities. Maximal movement appears at the resting level of $[Ca^{2+}]_c$, but complete suppression of mitochondrial motility occurs during agonist-induced $[Ca^{2+}]_c$ spikes and oscillations. The motor mechanism promptly responds to $[Ca^{2+}]_c$ increases and recovery follows the decay in $[Ca^{2+}]_c$, still the delay in recovery is sufficiently long to allow the motility inhibition spikes to run together during $[Ca^{2+}]_c$ oscillations. Thus, frequency-modulated $[Ca^{2+}]_c$ oscillations are particularly effective to exert dynamic control over mitochondrial motility. During the calcium signal, the mitochondrial motility also shows subcellular heterogeneity that reflects the spatial pattern of Ca²⁺ release. Depression of the movement results in immobilization and recruitment of the mitochondria in the vicinity of the most active Ca²⁺ release sites. We have also demonstrated that mitochondria preferentially localize to and move along the MTs. Movement of the mitochondria is likely to be primarily facilitated by dynein and kinesin, and the Ca²⁺ sensitivity of the motor mechanism is likely to be conferred by a distinct Ca²⁺ sensor molecule. Finally, we provided evidence that the propagation of Ca²⁺ spikes to the mitochondria is accelerated if mitochondrial motility is attenuated.

The scheme in Fig. 6 and the animation in Video 3 (available at http://www.jcb.org/cgi/content/full/jcb.200406038/DC1) show the mechanism of the Ca²⁺-dependent control of mitochondrial movement determined in the present work. At resting $[Ca^{2+}]_c$ (Fig. 6, left), mitochondria display maximal movement activity and the majority of the movements occur along the MTs (Fig. 6 left, arrows). Movements of the mitochondria toward the plus end are promoted by kinesin motors, whereas movements to the minus end are facilitated by dynein motor proteins (Tanaka et al., 1998; Habermann et al., 2001; Deacon et al., 2003; Varadi et al., 2004). When a $[Ca^{2+}]_c$ rise occurs due to either Ca²⁺ mobilization or Ca²⁺ entry, the mitochondrial movement decreases. Even a modest increase in $[Ca^{2+}]_c$ is sufficient to attenuate mitochondrial motility and the elevation of global $[Ca^{2+}]_c$ to 1 μM, a level that is commonly attained during $[Ca^{2+}]_c$ spikes and oscillations results in almost complete loss of mitochondrial movement (Video 3, right panel). Ca²⁺ does not seem to activate Ca²⁺/CaM-dependent kinases or the Ca²⁺-dependent protein phosphatase to establish control over mitochondrial motility because several inhibitors of these enzymes failed to interfere with the movement inhibition by Ca²⁺. Furthermore, Ca²⁺ does not seem to target directly the microtubular motors because the molecular structure of mammalian cytoplasmic dynein and kinesin does not indicate the presence of a site for binding of Ca²⁺ or CaM (Vale, 2003). Thus, we propose that a distinct Ca²⁺ sensor molecule is required to translate the Ca²⁺ signal for the microtubular motor proteins. Binding of Ca²⁺ to the Ca²⁺ sensor would induce the MT-bound motors to lock in a stationary position or to detach from the MTs (Video 3, red symbol). One potential candidate for the Ca²⁺ sensor is myosin Va, a motor protein that binds CaM and is controlled by Ca²⁺ (for reviews see Reck-Peterson

Figure 6. **Decoding of $[Ca^{2+}]_c$ signals by the mitochondrial motor machinery.** The proposed mechanism for the $[Ca^{2+}]_c$ signal-dependent control of mitochondrial motility is shown.
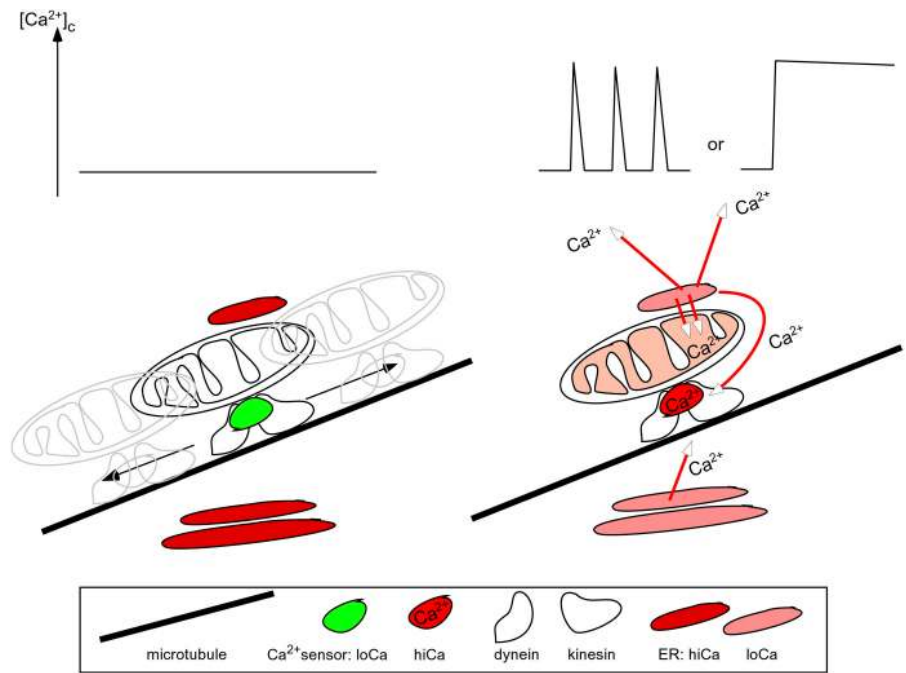
et al., 2000; Vale, 2003). Myosin Va displays a Ca^{2+}-dependent interaction with actin-filaments (Tauhata et al., 2001; Krementsov et al., 2004) and MTs (Cao et al., 2004). Interaction of the head domain of myosin Va with actin provides a motor for movement along the MFs but the tail domain-based interaction with MTs does not present by itself a microtubular motor. However, recent papers have raised the possibility that myosin V can interact directly with dynein and kinesin and through this interaction may affect motor function at the MTs (Benashski et al., 1997; Huang et al., 1999; Stafford et al., 2000; Lalli et al., 2003). Immunocytochemistry studies indicate that myosin Va is present on the mitochondria in H9c2 cells, and myosin Va is also retained on isolated mitochondria (unpublished data). However, to clarify the role of myosin V in the Ca^{2+}-dependent control of mitochondrial motility and to explore alternative mechanisms, further studies are needed.

A primary source of the $[Ca^{2+}]_c$ rise for $[Ca^{2+}]_c$ spikes and oscillations is Ca^{2+} mobilization from the ER/SR (Fig. 6, right). Ca^{2+} release from the ER appears to control the mitochondrial motility through elevation of the $[Ca^{2+}]_c$ (Fig. 6, long red arrows). The inhibition of movement appears almost instantaneously as the $[Ca^{2+}]_c$ rises and gradually and completely disappears after the decay of the $[Ca^{2+}]_c$ signal. Owing to the relatively slow recovery of mitochondrial motility, the attenuation of motility induced by a global $[Ca^{2+}]_c$ spike may persist until the rise of the next $[Ca^{2+}]_c$ spike during $[Ca^{2+}]_c$ oscillations (Video 3). However, the calcium signal is often spatially heterogeneous or Ca^{2+} release events remain confined and do not give rise to a global $[Ca^{2+}]_c$ signal. Based on our observation that the inhibition of the motility corresponds to the spatial pattern of the $[Ca^{2+}]_c$ rise (Fig. 4 C), the Ca^{2+}-induced inhibition of motility mitochondria appears to provide a mechanism to sustain mitochondria close to Ca^{2+} release sites that are particularly active. Interestingly, elevation of $[Ca^{2+}]_c$ to >1 μM

has been shown to cause enhanced association of the mitochondria with the ER in permeabilized cells (Wang et al., 2000). The dynamic positioning of the mitochondria may cooperate with permanent tethering structures (Filippin et al., 2003; unpublished data) to maintain the close associations between ER/SR Ca^{2+} release sites and the mitochondria (Rizzuto et al., 1998; Marchant et al., 2002; Pacher et al., 2002). Along this line, propagation of the calcium signal to the mitochondria, which appears to depend on the local communication between IP_3 receptors and mitochondrial Ca^{2+} uptake sites was more effective when mitochondrial movement was abolished by pretreatment with an MT-disruptive agent (Fig. 5 B). Thus, an important feature of the present model is the creation, by inhibition of movement, of the condition for a stable ER–mitochondrial interface that may facilitate the back-and-forth Ca^{2+} transport between ER and mitochondria. Freezing of mitochondria should be preceded by alignment of the mitochondrial Ca^{2+} uptake sites with the ER Ca^{2+} release sites, but this process was not possible to resolve by the present approaches.

Recruitment of mitochondria to the sites of Ca^{2+} release by Ca^{2+}-induced immobilization may form the basis for a novel homeostatic mechanism in calcium signaling. Targeting of mitochondria to the sites of Ca^{2+} release results in an increase in the local Ca^{2+} buffering capacity. Also, mitochondrial Ca^{2+} uptake serves as a means for stimulation of mitochondrial ATP production that provides a localized energy source for Ca^{2+} reuptake by the ER/SR (Landolfi et al., 1998). The increase in local Ca^{2+} buffering and in ATP production represents a feedback mechanism that contributes to the control of the $[Ca^{2+}]_c$ rise and strengthening of the Ca^{2+} scavenger mechanisms may also be important to avoid Ca^{2+}-dependent cell injury. Once Ca^{2+} release stops, motility is recovered and the mitochondria may be recruited by Ca^{2+} release in other regions of the cell. Thus, the Ca^{2+}-dependent control of mitochondrial

motility offers a means to adjust the subcellular spatial arrangements of the Ca^{2+} buffering and energy production as needed.

In conclusion, mitochondrial movement along the MTs ensures that mitochondria are available throughout the cell, whereas regulation by Ca^{2+} targets mitochondria to the sites where mitochondrial Ca^{2+} uptake and ATP production may be required to ensure the handling of Ca^{2+}. Dynamic control of mitochondrial motility and distribution presents a powerful, novel mechanism to optimize the use of the mitochondrial pool in cellular Ca^{2+} transport and signaling.

Materials and methods

Cells
H9c2 cells were cultured for 4 d in DME supplemented with 10% FBS, 2 mM glutamine, 1 mM pyruvate, 100 U/ml penicillin, and 100 µg/ml streptomycin in humidified air (5% CO_2) at 37°C. For imaging experiments, cells were plated onto poly-D-lysine–coated glass coverslips.

Transient expression
When the cell culture reached 70% confluency (2 d after plating), transfection was performed using Lipofectamine 2000 (Invitrogen) according to the manufacturer's instructions with 2 µg/ml of each vector. One or two of the vectors that encode pEYFP-mito, pDsRed-mito, pEGFP-tubulin, pEGFP-actin (BD Biosciences), or ratiometric-pericams targeted to the cytoplasm, nucleus, or mitochondria (provided by A. Miyawaki, RIKEN, Wako City, Japan) or RyR1 (a gift from J. Ma, University of Medicine and Dentistry of New Jersey, Piscataway, NJ) were used. Transfected cells were further incubated in the culture for 24–36 h before the imaging experiments.

Live cell imaging
Fluorescence imaging was performed using an inverted microscope (model IX70; Olympus; 40×, UApo340, NA 1.35) fitted with a cooled CCD camera (Pluto; Pixelvision) and a high speed wavelength switcher (model Lambda DG; Sutter Instruments) controlled by Spectralyzer (custom) software. Simultaneous detection of fura2 (340 and 380 nm excitation) and mitoYFP (495 nm excitation) fluorescence was achieved using a multiwavelength beamsplitter/emission filter combination (Chroma Technology Corp.). Pericam was excited at 415 and 495 nm. The data acquisition rate was 0.4 triplet per second in the fura2 and mitoYFP imaging and 2 duplet per second in the pericam imaging experiments. To correct for the camera noise, the dark (excitation path closed) image was obtained and was subtracted from each image.

Confocal imaging of the fluorescent proteins targeted to the mitochondria, MFs, and MTs was performed using an imaging system (model Radiance 2100; Bio-Rad Laboratories) equipped with a Kr/Ar-ion laser source (488 and 568 nm excitation) fitted to an inverted microscope (40×, UApo340, NA 1.35). Mitotracker green, GFP, and YFP were excited at 488 nm, and DsRed at 568 nm. Images were obtained every 3.1–3.3 s using LaserSharp software (Bio-Rad Laboratories).

To simultaneously measure $[Ca^{2+}]_c$ with mitochondrial motility, mitoYFP-transfected cell cultures were preincubated for 20 min in an extracellular medium (ECM; 2% BSA, 121 mM NaCl, 5 mM NaHCO3, 10 mM Na-Hepes, 4.7 mM KCl, 1.2 mM KH$_2$PO4, 1.2 mM MgSO$_4$, 2 mM CaCl$_2$, and 10 mM glucose, pH 7.4), and then loaded with 5 µM fura2/AM for 25–30 min at RT in the presence of 0.003% (wt/vol) pluronic acid and 200 µM sulfinpyrazone. After washing of the dye-loaded cells, imaging measurements were performed in ECM containing 0.25% BSA at 35°C. Imaging of pericam, mitoYFP, actinGFP+mitoDsRed, and tubulin-GFP+mitoDsRed was also performed in 0.25% BSA-ECM at 35°C.

To calibrate the changes in $[Ca^{2+}]_c$, the ratio of 340/380 nm fluorescence values was calculated for the fura2-loaded cells after subtraction of background fluorescence. The ratio was converted to nanomole values using in vitro calibration of fura2-free acid (K_d = 224 nM). To quantitate mitochondrial motility a difference image protocol was used. By subtraction of sequential images, the fluorescence change for each pixel was calculated, and then pixels that exhibited a change after 3 × 3 median filtering (positive or negative) greater than an empirically determined threshold (2.5% of the mean fluorescence intensity/pixel) were counted for each time point. Changes in the pixel number were normalized to the initial value calculated for cells before stimulation.

All image analysis was done in Spectralyzer imaging software. Experiments were performed with ≥3 different cell preparations. Traces represent single cell responses unless indicated otherwise. Data are presented as means ± SEM. Significance of differences from the relevant controls was calculated by t test.

Online supplemental material
Video 1 shows the inhibition of mitochondrial motility in an H9c2 cell stimulated with VP; Video 2 demonstrates the movement of mitochondria along MTs; and Video 3 is an animated representation of the proposed mechanism for calcium control of mitochondrial motility. Online supplemental material is available at http://www.jcb.org/cgi/content/full/jcb.200406038/DC1.

References

Ball, E.H., and S.J. Singer. 1982. Mitochondria are associated with microtubules and not with intermediate filaments in cultured fibroblasts. *Proc. Natl. Acad. Sci. USA.* 79:123–126.

Bhat, M.B., J. Zhao, W. Zang, C.W. Balke, H. Takeshima, W.G. Wier, and J. Ma. 1997. Caffeine-induced release of intracellular Ca^{2+} from Chinese hamster ovary cells expressing skeletal muscle ryanodine receptor. Effects on full-length and carboxyl-terminal portion of Ca^{2+} release channels. *J. Gen. Physiol.* 110:749–762.

Benashski, S.E., A. Harrison, R.S. Patel-King, and S.M. King. 1997. Dimerization of the highly conserved light chain shared by dynein and myosin V. *J. Biol. Chem.* 272:20929–20935.

Bernardi, P., V. Petronilli, F. Di Lisa, and M. Forte. 2001. A mitochondrial perspective on cell death. *Trends Biochem. Sci.* 26:112–117.

Cao, T.T., W. Chang, S.E. Masters, and M.S. Mooseker. 2004. Myosin-Va binds to and mechanochemically couples microtubules to actin filaments. *Mol. Biol. Cell.* 15:151–161.

Collins, T.J., P. Lipp, M.J. Berridge, and M.D. Bootman. 2001. Mitochondrial Ca^{2+} uptake depends on the spatial and temporal profile of cytosolic Ca^{2+} signals. *J. Biol. Chem.* 276:26411–26420.

Couchman, J.R., and D.A. Rees. 1982. Organelle-cytoskeleton relationships in fibroblasts: mitochondria, Golgi apparatus, and endoplasmic reticulum in phases of movement and growth. *Eur. J. Cell Biol.* 27:47–54.

Csordás, G., and G. Hajnóczky. 2003. Plasticity of mitochondrial calcium signaling. *J. Biol. Chem.* 278:42273–42282.

Csordás, G., A.P. Thomas, and G. Hajnóczky. 1999. Quasi-synaptic calcium signal transmission between endoplasmic reticulum and mitochondria. *EMBO J.* 18:96–108.

Deacon, S.W., A.S. Serpinskaya, P.S. Vaughan, M. Lopez Fanarraga, I. Vernos, K.T. Vaughan, and V.I. Gelfand. 2003. Dynactin is required for bidirectional organelle transport. *J. Cell Biol.* 160:297–301.

Demaurex, N., and C. Distelhorst. 2003. Cell biology. Apoptosis–the calcium connection. *Science.* 300:65–67.

De Vos, K.J., J. Sable, K.E. Miller, and M.P. Sheetz. 2003. Expression of phosphatidylinositol (4,5) bisphosphate-specific pleckstrin homology domains alters direction but not the level of axonal transport of mitochondria. *Mol. Biol. Cell.* 14:3636–3649.

Drubin, D.G., H.D. Jones, and K.F. Wertman. 1993. Actin structure and function: roles in mitochondrial organization and morphogenesis in budding yeast and identification of the phalloidin-binding site. *Mol. Biol. Cell.* 4:1277–1294.

Duchen, M.R. 2000. Mitochondria and calcium: from cell signalling to cell death. *J. Physiol.* 529:57–68.

Filippin, L., P.J. Magalhaes, G. Di Benedetto, M. Colella, and T. Pozzan. 2003. Stable interactions between mitochondria and endoplasmic reticulum allow rapid accumulation of calcium in a subpopulation of mitochondria. *J. Biol. Chem.* 278:39224–39234.

Habermann, A., T.A. Schroer, G. Griffiths, and J.K. Burkhardt. 2001. Immunolocalization of cytoplasmic dynein and dynactin subunits in cultured macrophages: enrichment on early endocytic organelles. *J. Cell Sci.* 114:229–240.

Hajnóczky, G., L.D. Robb-Gaspers, M. Seitz, and A.P. Thomas. 1995. Decoding

of cytosolic calcium oscillations in the mitochondria. *Cell.* 82:415–424.

Hajnóczky, G., G. Csordás, and M. Yi. 2002. Old players in a new role: mitochondria-associated membranes, VDAC, and ryanodine receptors as contributors to calcium signal propagation from endoplasmic reticulum to the mitochondria. *Cell Calcium.* 32:363–377.

Hoth, M., C.M. Fanger, and R.S. Lewis. 1997. Mitochondrial regulation of store-operated calcium signaling in T lymphocytes. *J. Cell Biol.* 137:633–648.

Huang, J.D., S.T. Brady, B.W. Richards, D. Stenolen, J.H. Resau, N.G. Copeland, and N.A. Jenkins. 1999. Direct interaction of microtubule- and actin-based transport motors. *Nature.* 397:267–270.

Jacobson, J., and M.R. Duchen. 2001. 'What nourishes me, destroys me': towards a new mitochondrial biology. *Cell Death Differ.* 8:963–966.

Khodjakov, A., E.M. Lizunova, A.A. Minin, M.P. Koonce, and F.K. Gyoeva. 1998. A specific light chain of kinesin associates with mitochondria in cultured cells. *Mol. Biol. Cell.* 9:333–343.

Krementsov, D.N., E.B. Krementsova, and K.M. Trybus. 2004. Myosin V: regulation by calcium, calmodulin, and the tail domain. *J. Cell Biol.* 164:877–886.

Kroemer, G., and J.C. Reed. 2000. Mitochondrial control of cell death. *Nat. Med.* 6:513–519.

Lalli, G., S. Gschmeissner, and G. Schiavo. 2003. Myosin Va and microtubule-based motors are required for fast axonal retrograde transport of tetanus toxin in motor neurons. *J. Cell Sci.* 116:4639–4650.

Landolfi, B., S. Curci, L. Debellis, T. Pozzan, and A.M. Hofer. 1998. Ca^{2+} homeostasis in the agonist-sensitive internal store: functional interactions between mitochondria and the ER measured in situ in intact cells. *J. Cell Biol.* 142:1235–1243.

Lawrie, A.M., R. Rizzuto, T. Pozzan, and A.W. Simpson. 1996. A role for calcium influx in the regulation of mitochondrial calcium in endothelial cells. *J. Biol. Chem.* 271:10753–10759.

Marchant, J.S., V. Ramos, and I. Parker. 2002. Structural and functional relationships between Ca^{2+} puffs and mitochondria in *Xenopus* oocytes. *Am. J. Physiol. Cell Physiol.* 282:C1374–C1386.

Martinou, J.C., and D.R. Green. 2001. Breaking the mitochondrial barrier. *Nat. Rev. Mol. Cell Biol.* 2:63–67.

Montero, M., M.T. Alonso, E. Carnicero, I. Cuchillo-Ibanez, A. Albillos, A.G. Garcia, J. Garcia-Sancho, and J. Alvarez. 2000. Chromaffin-cell stimulation triggers fast millimolar mitochondrial Ca^{2+} transients that modulate secretion. *Nat. Cell Biol.* 2:57–61.

Morris, R.L., and P.J. Hollenbeck. 1995. Axonal transport of mitochondria along microtubules and F-actin in living vertebrate neurons. *J. Cell Biol.* 131:1315–1326.

Nagai, T., A. Sawano, E.S. Park, and A. Miyawaki. 2001. Circularly permuted green fluorescent proteins engineered to sense Ca^{2+}. *Proc. Natl. Acad. Sci. USA.* 98:3197–3202.

Nangaku, M., R. Sato-Yoshitake, Y. Okada, Y. Noda, R. Takemura, H. Yamazaki, and N. Hirokawa. 1994. KIF1B, a novel microtubule plus end-directed monomeric motor protein for transport of mitochondria. *Cell.* 79:1209–1220.

Pacher, P., and G. Hajnóczky. 2001. Propagation of the apoptotic signal by mitochondrial waves. *EMBO J.* 20:4107–4121.

Pacher, P., A.P. Thomas, and G. Hajnóczky. 2002. Ca^{2+} marks: miniature calcium signals in single mitochondria driven by ryanodine receptors. *Proc. Natl. Acad. Sci. USA.* 99:2380–2385.

Parekh, A.B. 2003. Store-operated Ca^{2+} entry: dynamic interplay between endoplasmic reticulum, mitochondria and plasma membrane. *J. Physiol.* 547:333–348.

Park, M.K., M.C. Ashby, G. Erdemli, O.H. Petersen, and A.V. Tepikin. 2001. Perinuclear, perigranular and sub-plasmalemmal mitochondria have distinct functions in the regulation of cellular calcium transport. *EMBO J.* 20:1863–1874.

Petersen, O.H. 2002. Calcium signal compartmentalization. *Biol. Res.* 35:177–182.

Reck-Peterson, S.L., D.W. Provance Jr., M.S., Mooseker, and J.A. Mercer. 2000. Class V myosins. *Biochim. Biophys. Acta.* 1496:36–51.

Rintoul, G.L., A.J. Filiano, J.B. Brocard, G.J. Kress, and I.J. Reynolds. 2003. Glutamate decreases mitochondrial size and movement in primary forebrain neurons. *J. Neurosci.* 23:7881–7888.

Rizzuto, R., M. Brini, M. Murgia, and T. Pozzan. 1993. Microdomains with high Ca^{2+} close to IP$_3$-sensitive channels that are sensed by neighboring mitochondria. *Science.* 262:744–747.

Rizzuto, R., P. Pinton, W. Carrington, F.S. Fay, K.E. Fogarty, L.M. Lifshitz, R.A. Tuft, and T. Pozzan. 1998. Close contacts with the endoplasmic reticulum as determinants of mitochondrial Ca^{2+} responses. *Science.* 280:1763–1766.

Rizzuto, R., P. Bernardi, and T. Pozzan. 2000. Mitochondria as all-round players of the calcium game. *J. Physiol.* 529:37–47.

Rizzuto, R., M.R. Duchen, and T. Pozzan. 2004. Flirting in little space: the ER/mitochondria Ca^{2+} liaison. *Sci. STKE.* 2004:re1.

Robb-Gaspers, L.D., P. Burnett, G.A. Rutter, R.M. Denton, R. Rizzuto, and A.P. Thomas. 1998. Integrating cytosolic calcium signals into mitochondrial metabolic responses. *EMBO J.* 17:4987–5000.

Scorrano, L., and S.J. Korsmeyer. 2003. Mechanisms of cytochrome c release by proapoptotic BCL-2 family members. *Biochem. Biophys. Res. Commun.* 304:437–444.

Stafford, P., J. Brown, and G.M. Langford. 2000. Interaction of actin- and microtubule-based motors in squid axoplasm probed with antibodies to myosin V and kinesin. *Biol. Bull.* 199:203–205.

Stromer, M.H., and M. Bendayan. 1990. Immunocytochemical identification of cytoskeletal linkages to smooth muscle cell nuclei and mitochondria. *Cell Motil. Cytoskeleton.* 17:11–18.

Szalai, G., G. Csordás, B. Hantash, A.P. Thomas, and G. Hajnóczky. 2000. Calcium signal transmission between ryanodine receptors and mitochondria. *J. Biol. Chem.* 275:15305–15313.

Summerhayes, I.C., D. Wong, and L.B. Chen. 1983. Effect of microtubules and intermediate filaments on mitochondrial distribution. *J. Cell Sci.* 61:87–105.

Tanaka, Y., Y. Kanai, Y. Okada, S. Nonaka, S. Takeda, A. Harada, and N. Hirokawa. 1998. Targeted disruption of mouse conventional kinesin heavy chain, kif5B, results in abnormal perinuclear clustering of mitochondria. *Cell.* 93:1147–1158.

Tauhata, S.B., D.V. dos Santos, E.W. Taylor, M.S. Mooseker, and R.E. Larson. 2001. High affinity binding of brain myosin-Va to F-actin induced by calcium in the presence of ATP. *J. Biol. Chem.* 276:39812–39818.

Vale, R.D. 2003. The molecular motor toolbox for intracellular transport. *Cell.* 112:467–480.

Varadi, A., L.I. Johnson-Cadwell, V. Cirulli, Y. Yoon, V.J. Allan, and G.A. Rutter. 2004. Cytoplasmic dynein regulates the subcellular distribution of mitochondria by controlling the recruitment of the fission factor dynamin-related protein-1. *J. Cell Sci.* 117:4389–4400.

Wang, H.J., G. Guay, L. Pogan, R. Sauve, and I.R. Nabi. 2000. Calcium regulates the association between mitochondria and a smooth subdomain of the endoplasmic reticulum. *J. Cell Biol.* 150:1489–1498.

Yaffe, M.P. 1999. Dynamic mitochondria. *Nat. Cell Biol.* 1:E149–E150.